SCIENTIFIC REPORTS
natureresearch

Check for updates

OPEN

Hybrid nanofluid flow towards a stagnation point on a stretching/shrinking cylinder

Iskandar Waini[1,2], Anuar Ishak[2] ✉ & Ioan Pop[3]

This paper examines the stagnation point flow towards a stretching/shrinking cylinder in a hybrid nanofluid. Here, copper (Cu) and alumina (Al_2O_3) are considered as the hybrid nanoparticles while water as the base fluid. The governing equations are reduced to the similarity equations using a similarity transformation. The resulting equations are solved numerically using the boundary value problem solver, bvp4c, available in the Matlab software. It is found that the heat transfer rate is greater for the hybrid nanofluid compared to the regular nanofluid as well as the regular fluid. Besides, the non-uniqueness of the solutions is observed for certain physical parameters. It is also noticed that the bifurcation of the solutions occurs in the shrinking regions. In addition, the heat transfer rate and the skin friction coefficients increase in the presence of nanoparticles and for larger Reynolds number. It is found that between the two solutions, only one of them is stable as time evolves.

Boundary layer flow caused by the stretching/shrinking surface has been practiced in industrial engineering and manufacturing processes. To name a few, the polymer or metal extrusions, wire drawing, and continuous glass casting are such processes that involved these kinds of surfaces[1,2]. Historically, it seems that Crane[3] is the first researcher to examine the flow over a linearly stretching surface. Instead of a stretching surface, the problems of a shrinking surface have become the topic of interest in the last few years. The flow caused by the shrinking surface is fundamentally a reverse flow as pondered by Goldstein[4]. This type of flow is different from the stretching surface owing to the existence of the vorticity inside the boundary layer, which discovered by Wang[5]. Thus, some other outside force is required to overcome this situation and only then the steady flow is possible. In the work of Miklavčič and Wang[6], they suggested that the flow can be preserved by the application of suction on the surface. Besides, the existence of the stagnation flow velocity can confine the vorticity to maintain the flow, thus the application of suction on the shrinking sheet is not necessary as discussed by Wang[7]. The stagnation point flow describes the fluid movement close to the stagnation region of a solid surface.

The problem of stagnation point flow towards a cylinder has been also considered by many researchers. For example, Wang[8] considered the stagnation flow towards a circular cylinder. Then, Wang[9] extended this problem by considering partial slip condition on the cylinder surface. After that, Gorla[10] examined a similar problem of Wang[8] but with the effect of Prandtl numbers on the heat transfer. Then, Cunning et al.[11] investigated the transpiration and rotation effects on the stagnation flow towards a circular cylinder. However, there is a limited reference on the flow over a shrinking cylinder in the literature. In this respect, Lok and Pop[12] investigated this problem by considering the stagnation point flow and suction effects. Merkin et al.[13] studied the stagnation-point flow and heat transfer over an exponentially stretching/shrinking cylinder. Further, Zaimi et al.[14] examined the effect of suction on the unsteady flow over a shrinking cylinder and found the dual solutions exist for a certain range of suction and unsteadiness parameters. Besides, Soomro et al.[15] examined the nanofluid flow along a permeable shrinking vertical cylinder with slip effects. Other than that, some other useful studies to simulate the flow over a cylinder under different conditions can be found in the literature[16–21].

Nowadays, the problem of heat transfer enhancement in industrial processes has become the main topic of interest to the researchers. Previously, the fluids like water, oil, and ethylene glycol were regularly considered as a cooling liquid in those processes, but their heat transfer rates are low. In 1995, Choi and Eastman[22] introduced the fluid called 'nanofluid' to replace the use of regular fluids in the industrial processes. Nanofluids are engineered by

[1]Fakulti Teknologi Kejuruteraan Mekanikal dan Pembuatan, Universiti Teknikal Malaysia Melaka, Hang Tuah Jaya, 76100 Durian Tunggal, Melaka, Malaysia. [2]Department of Mathematical Sciences, Faculty of Science and Technology, Universiti Kebangsaan Malaysia, 43600 UKM, Bangi, Selangor, Malaysia. [3]Department of Mathematics, Babeş-Bolyai University, 400084, Cluj-Napoca, Romania. ✉e-mail: anuar_mi@ukm.edu.my
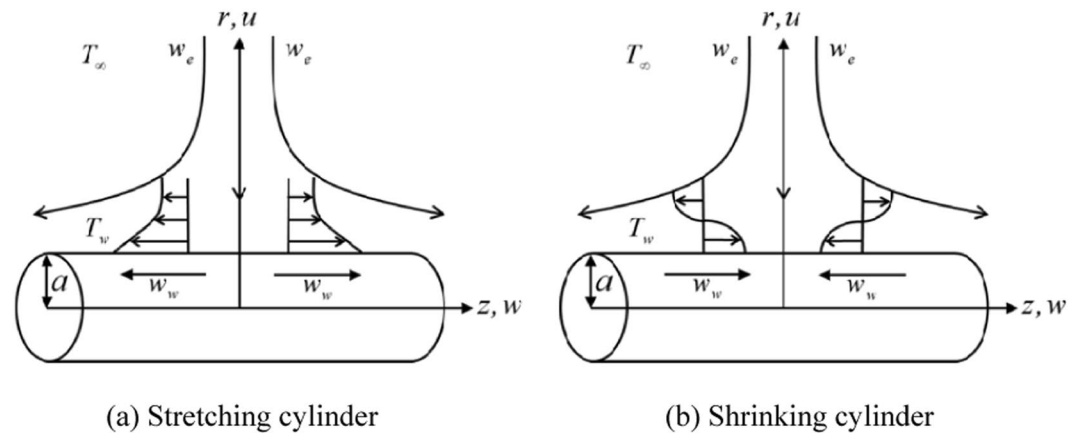
Figure 1. Physical configuration.

dispersing one type of nanoparticle in the aforementioned fluids to enhance their thermal conductivity. Khanafer et al.[23] and Oztop and Abu-Nada[24] have utilized nanofluids to study the heat transfer enhancement in a rectangular enclosure. However, the researchers found that the thermal properties of the nanofluid could be improved with the addition of more than a single nanoparticle in the base fluid and named it 'hybrid nanofluid'. The experimental studies that considered the hybrid nano-composite particles have been conducted by several researchers, for example, Turcu et al.[25] and Jana et al.[26]. Hybrid nanofluid is an advanced fluid that incorporates more than one nanoparticle which has the capacity of raising the heat transfer rate because of the synergistic effects[27].

Furthermore, the studies of hybrid nanofluid were extended to the boundary layer flow problem. For instance, Devi and Devi[28,29] started to examine the advantages of utilizing hybrid nanofluid over a stretching surface. They found that the heat transfer rate was intensified in the presence of the hybrid nanoparticles. In their studies, the new thermophysical model was introduced and validated with the experimental data of Suresh et al.[30]. Furthermore, Waini et al.[31] examined the stability of the multiple solutions of the flow over a stretching/shrinking surface in a fluid containing hybrid nanoparticles. They discovered that only one of the solutions is stable and thus physically reliable as time evolves. Besides, Waini et al.[32–37] in a series of papers have extended the problem to different surfaces. Moreover, the effects of MHD and viscous dissipation have been studied by Lund et al.[38], considering Cu–Fe_3O_4/H_2O hybrid nanofluid in a porous medium. Additionally, the problem of hybrid nanofluid flow with the effect of different physical parameters was also considered by several authors[39–45].

Thus, the objective of this paper is to examine the hybrid nanofluid flow towards a stagnation point on a stretching/shrinking cylinder. Here, copper (Cu) and alumina (Al_2O_3) are considered as the hybrid nanoparticles, while water as the base fluid.

Mathematical Model

Consider a hybrid nanofluid flow towards a stagnation point on a stretching/shrinking cylinder with radius a as illustrated in Fig. 1. Here, (z,r) is the cylindrical polar coordinates which assigned in the axial and radial directions, respectively. The flow is assumed to be symmetric about the $z = 0$ plane and also axisymmetric about the z-axis, with the stagnation line is at $z = 0$ and $r = a$. The surface velocity of the cylinder is given as $w_w(z) = 2bz$ where the static cylinder is denoted by $b = 0$, whereas the cylinder is stretched or shrunk when $b > 0$ or $b < 0$, respectively. Meanwhile, the free stream velocity is taken as $w_e(z) = 2cz$ where $c > 0$. Moreover, the surface temperature T_w and the ambient temperature T_∞ are constant, where $T_w > T_\infty$. Also, it is assumed that the shape of the nanoparticle is spherical and its size is uniform, while the agglomeration is disregarded since the hybrid nanofluid is formed as a stable composite. Therefore, the equations that govern the hybrid nanofluid flow are (see Wang[8], Lok and Pop[12]):

$$\frac{\partial(rw)}{\partial z} + \frac{\partial(ru)}{\partial r} = 0 \tag{1}$$

$$w\frac{\partial w}{\partial z} + u\frac{\partial w}{\partial r} = w_e\frac{dw_e}{dz} + \frac{\mu_{hnf}}{\rho_{hnf}}\left(\frac{\partial^2 w}{\partial r^2} + \frac{1}{r}\frac{\partial w}{\partial r}\right) \tag{2}$$

$$w\frac{\partial T}{\partial z} + u\frac{\partial T}{\partial r} = \frac{k_{hnf}}{\left(\rho C_p\right)_{hnf}}\left(\frac{\partial^2 T}{\partial r^2} + \frac{1}{r}\frac{\partial T}{\partial r}\right) \tag{3}$$

subject to:

$$u = 0, \; w = w_w, \; T = T_w \text{ at } r = a$$

Thermophysical Properties	Nanofluid	Hybrid nanofluid
Density	$\rho_{nf} = (1 - \varphi_1)\rho_f + \varphi_1\rho_{n1}$	$\rho_{hnf} = (1 - \varphi_2)\left[(1 - \varphi_1)\rho_f + \varphi_1\rho_{n1}\right] + \varphi_2\rho_{n2}$
Heat capacity	$(\rho C_p)_{nf} = (1 - \varphi_1)(\rho C_p)_f + \varphi_1(\rho C_p)_{n1}$	$(\rho C_p)_{hnf} = (1 - \varphi_2)\left[(1 - \varphi_1)(\rho C_p)_f + \varphi_1(\rho C_p)_{n1}\right] + \varphi_2(\rho C_p)_{n2}$
Dynamic viscosity	$\mu_{nf} = \dfrac{\mu_f}{(1 - \varphi_1)^{2.5}}$	$\mu_{hnf} = \dfrac{\mu_f}{(1 - \varphi_1)^{2.5}(1 - \varphi_2)^{2.5}}$
Thermal conductivity	$\dfrac{k_{nf}}{k_f} = \dfrac{k_{n1} + 2k_f - 2\varphi_1(k_f - k_{n1})}{k_{n1} + 2k_f + \varphi_1(k_f - k_{n1})}$	$\dfrac{k_{hnf}}{k_{nf}} = \dfrac{k_{n2} + 2k_{nf} - 2\varphi_2(k_{nf} - k_{n2})}{k_{n2} + 2k_{nf} + \varphi_2(k_{nf} - k_{n2})}$ where $\dfrac{k_{nf}}{k_f} = \dfrac{k_{n1} + 2k_f - 2\varphi_1(k_f - k_{n1})}{k_{n1} + 2k_f + \varphi_1(k_f - k_{n1})}$

Table 1. Thermophysical properties of nanofluid and hybrid nanofluid[24,28,31].

Thermophysical Properties	Al$_2$O$_3$	Cu	water
$\rho(kg/m^3)$	3970	8933	997.1
$C_p(J/kgK)$	765	385	4179
$k(W/mK)$	40	400	0.613
Prandtl number, Pr			6.2

Table 2. Thermophysical properties of nanoparticles and water[24,31].

$$w \to w_e, \ T \to T_\infty \text{ as } r \to \infty \tag{4}$$

where w and u represent the velocity components along the z- and r- axes, and T represents the temperature of the hybrid nanofluid. Further, the thermophysical properties of the hybrid nanofluid are defined in Table 1 [24,28,31]. Besides, the physical properties of Al$_2$O$_3$, Cu, and water are provided in Table 2 [24,31]. Here, Al$_2$O$_3$ and Cu volume fractions are given by φ_1 and φ_2 and the subscripts $n1$ and $n2$ correspond to their solid components, respectively. Meanwhile, the fluid, nanofluid, and the hybrid nanofluid are designated by the subscripts f, nf, and hnf, respectively.

An appropriate transformation is introduced as follows (see Wang[8], Lok and Pop[12]):

$$u = - caf(\eta)/\sqrt{\eta}, \ w = 2czf'(\eta), \ \theta(\eta) = \frac{T - T_\infty}{T_w - T_\infty}, \ \eta = \left(\frac{r}{a}\right)^2 \tag{5}$$

Employing these definitions, Eq. (1) is identically fulfilled. Then, the following similarity equations are obtained:

$$\frac{\mu_{hnf}/\mu_f}{\rho_{hnf}/\rho_f}\left(\eta f'' + f''\right) + Re\left(ff'' - f'^2 + 1\right) = 0 \tag{6}$$

$$\frac{1}{Pr}\frac{k_{hnf}/k_f}{(\rho C_p)_{hnf}/(\rho C_p)_f}\left(\eta\theta'' + \theta'\right) + Re f\theta' = 0 \tag{7}$$

subject to:

$$f(1) = 0, f'(1) = \varepsilon, \theta(1) = 1$$

$$f'(\infty) = 1, \theta(\infty) = 0 \tag{8}$$

where ($'$) represents the differentiation with respect to η, $Re = ca^2/2\nu_f$ represents the Reynolds number, and $Pr = \mu_f(C_p)_f/k_f$ represents the Prandtl number. Besides, the stretching/shrinking parameter symbolized by $\varepsilon = b/c$ with $\varepsilon > 0$ and $\varepsilon < 0$ are for stretching and shrinking cylinder, respectively, while the static cylinder is denoted by $\varepsilon = 0$.

The skin friction coefficient C_f and the Nusselt number Nu are defined as:

Re	f″(1)				f) -2θ'(1)
	Wang[8]	Wang[9]	Lok and Pop[12]	Present results	Present results
0.2	0.78605	0.78604	0.786042	0.786042	1.508635
1	1.484185	1.48418	1.484183	1.484183	2.793424
10	4.16292	4.16292	4.162920	4.162920	7.701472

Table 3. Values of f″(1) and $-2\theta'(1)$ under different values of Re for regular fluid ($\varphi_1 = \varphi_2 = 0$) when $\varepsilon = 0$ and Pr=6.2.

$$C_f = \frac{2\mu_{hnf}}{\rho_f \, w_e^2}\left(\frac{\partial w}{\partial r}\right)_{r=a}, \quad Nu = -\frac{a \, k_{hnf}}{k_f\left(T_w - T_\infty\right)}\left(\frac{\partial T}{\partial r}\right)_{r=a} \tag{9}$$

Inserting (5) into (9), one obtains

$$\left(\frac{Rez}{a}\right)C_f = \frac{\mu_{hnf}}{\mu_f}f''(1), \quad Nu = -2\frac{k_{hnf}}{k_f}\theta'\left(1\right) \tag{10}$$

Stability Analysis

The existence of the non-uniqueness solutions of Eqs. (6) to (8) is observed for a certain range of the physical parameters. A temporal stability analysis is therefore needed to determine which solution is stable and thus physically reliable as time evolves. This technique was initiated by Merkin[46] in 1986. A dimensionless time variable τ was introduced by Weidman et al.[47] to further study the stability of the solutions in the long run. They concluded that the upper branch (first) solutions are stable, while the lower branch (second) solutions are unstable. The new variables based on Eq. (5) are given as follows:

$$u = -caf(\eta, \tau)/\sqrt{\eta}, \, w = 2cz\frac{\partial f}{\partial \eta}(\eta, \tau), \, \theta(\eta, \tau) = \frac{T - T_\infty}{T_w - T_\infty}, \, \eta = \left(\frac{r}{a}\right)^2, \, \tau = 2ct \tag{11}$$

To study the stability of the solutions of Eqs. (1) to (3), the unsteady form of these equations are considered. Using (11) and following the same procedure as previous section, the equations transformed to:

$$\frac{\mu_{hnf}/\mu_f}{\rho_{hnf}/\rho_f}\left(\eta\frac{\partial^3 f}{\partial \eta^3} + \frac{\partial^2 f}{\partial \eta^2}\right) + Re\left\{f\frac{\partial^2 f}{\partial \eta^2} - \left(\frac{\partial f}{\partial \eta}\right)^2 + 1 - \frac{\partial^2 f}{\partial \eta \partial \tau}\right\} = 0 \tag{12}$$

$$\frac{1}{Pr}\frac{k_{hnf}/k_f}{\left(\rho C_p\right)_{hnf}/\left(\rho C_p\right)_f}\left(\eta\frac{\partial^2 \theta}{\partial \eta^2} + \frac{\partial \theta}{\partial \eta}\right) + Re\left\{f\frac{\partial \theta}{\partial \eta} - \frac{\partial \theta}{\partial \tau}\right\} = 0 \tag{13}$$

subject to:

$$f(1, \tau) = 0, \frac{\partial f}{\partial \eta}\left(1, \tau\right) = \varepsilon, \theta(1, \tau) = 1$$

$$\frac{\partial f}{\partial \eta}(\infty, \tau) = 1, \theta\left(\infty, \tau\right) = 0 \tag{14}$$

To examine the stability behaviour, the disturbance is imposed to the steady solution $f = f_0(\eta)$ and $\theta = \theta_0(\eta)$ of Eqs. (6) to (8) by using the following relations (see Weidman et al.[47]):

$$f(\eta, \tau) = f_0(\eta) + e^{-\gamma\tau}F(\eta), \theta(\eta, \tau) = \theta_0(\eta) + e^{-\gamma\tau}G(\eta) \tag{15}$$

where γ indicates the unknown eigenvalue that determines the stability of the solutions, whereas $F(\eta)$ and $G(\eta)$ are small compared to $f_0(\eta)$ and $\theta_0(\eta)$. The disturbance is taken exponentially as it demonstrates the rapid decline or development of the disturbance. By employing Eq. (15), Eqs. (12) and (13) become

$$\frac{\mu_{hnf}/\mu_f}{\rho_{hnf}/\rho_f}(\eta F'' + F') + Re(f_0 F'' + f''_0 F - 2f'_0 F' + \gamma F') = 0 \tag{16}$$

φ_2	Re	ε	Cu/water ($\varphi_1 = 0$)		Al$_2$O$_3$-Cu/water ($\varphi_1 = 0.04$)	
			$(Rez/a)C_f$	Nu	$(Rez/a)C_f$	Nu
0	0.2	0	0.786042	1.508635	0.873892	1.632938
0.02			0.856892	1.584409	0.946858	1.712793
0.04			0.928449	1.660081	1.021036	1.792922
0.04	0.5		1.326543	2.330191	1.457949	2.509315
	1		1.769560	3.072779	1.944092	3.302625
	2		2.391980	4.113770	2.627041	4.414274
	1	-0.5	2.266010	2.074241	2.490374	2.279514
		0.5	0.994933	3.924611	1.092842	4.177081
		1.5	-1.181197	5.325017	-1.297131	5.621329

Table 4. Values of $(Rez/a)C_f$ and Nu for Cu/water ($\varphi_1 = 0$) and Al$_2$O$_3$-Cu/water ($\varphi_1 = 0.04$) under different values of physical parameters. when $Pr = 6.2$.
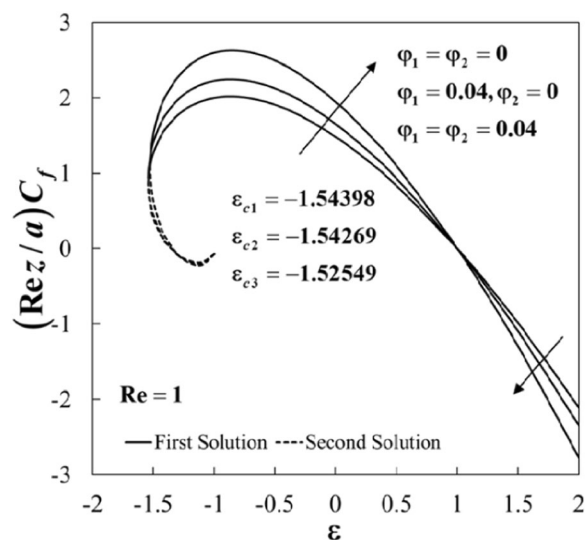
Figure 2. Plot of $(Re\,z/a)C_f$ against ε for different values of φ_1 and φ_2.

$$\frac{1}{Pr}\frac{k_{hnf}/k_f}{(\rho C_p)_{hnf}/(\rho C_p)_f}(\eta G'' + G') + Re(f_0 G' + \theta'_0 F + \gamma G) = 0 \tag{17}$$

subject to:

$$F(1) = 0,\ F'(1) = 0,\ G(1) = 0$$

$$F'(\infty) = 0,\ G(\infty) = 0 \tag{18}$$

Without loss of generality, the values of γ from Eqs. (16) to (18) are obtained for the case of $F''(1) = 1$ as proposed by Harris et al.[48].

Numerical Method

The boundary value problem solver, bvp4c, available in the Matlab software is utilized for solving Eqs. (6) to (8), numerically. As described in Shampine et al.[49], the aforementioned solver is a finite difference method that employs the 3-stage Lobatto IIIa formula. The selection of the initial guess and the boundary layer thickness η_∞ depend on the parameter values applied to obtain the required solutions. Moreover, several researchers[50–55] were also employing this solver for solving the boundary layer flow problems. First, Eqs. (6) and (7) are reduced to a system of ordinary differential equations of the first order. Equation (6) is written as:

$$f = y(1)$$

$$f' = y'(1) = y(2) \tag{19a}$$
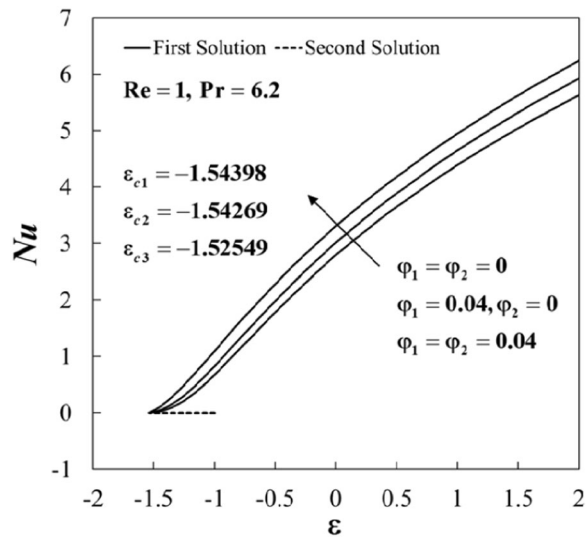
Figure 3. Plot of Nu against ε for different values of φ_1 and φ_2.
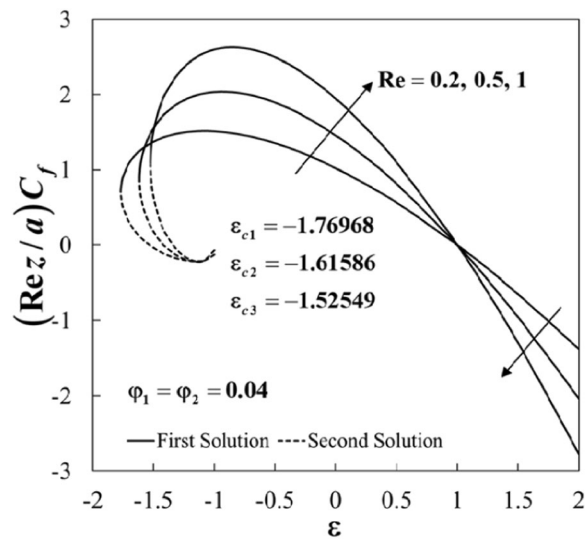
Figure 4. Plot of $(Rez/a)C_f$ against ε for different values of Re.

$$f'' = y'(2) = y(3) \tag{19b}$$

$$f''' = y'\left(3\right) = -\frac{1}{\eta}\left[\frac{\rho_{hnf}/\rho_f}{\mu_{hnf}/\mu_f}Re\left(y\left(1\right)y\left(3\right) - y(2)^2 + 1\right) + y\left(3\right)\right] \tag{19c}$$

while Eq. (7) becomes

$$\theta = y(4)$$

$$\theta' = y'(4) = y(5) \tag{20a}$$
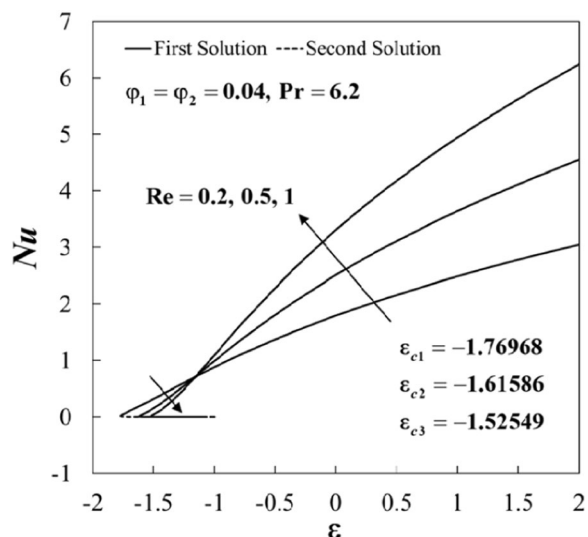
Figure 5. Plot of Nu against ε for different values of Re.
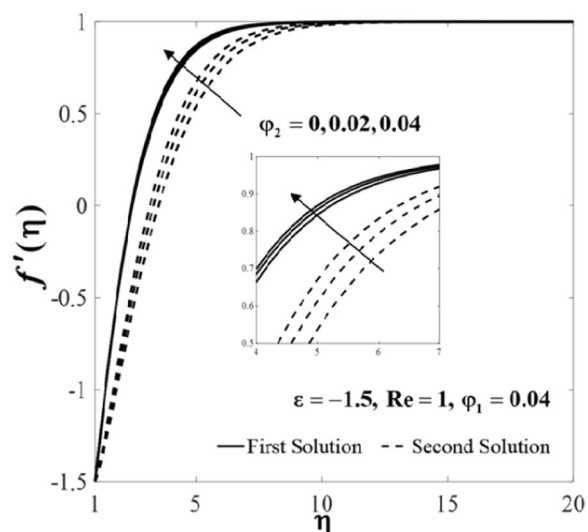
Figure 6. Plot of $f'(\eta)$ for different values of φ_2.

$$\theta'' = y'(5) = -\frac{1}{\eta}\left\{Pr\frac{(\rho C_p)_{hnf}/(\rho C_p)_f}{k_{hnf}/k_f}Rey\left(1\right)\left[y\left(5\right)\right] + y\left(5\right)\right\}$$

(20b)

with the boundary conditions:

$$ya(1) = 0, \ ya(2) = \varepsilon, \ ya(4) = 1$$

$$yb(2) = 1, \ yb(4) = 0$$

(21)

Then, Eqs. (19) to (21) are coded in Matlab software to obtain the required solutions.

Results and Discussion

In the present study, the volume fractions of Cu are varied from 0 to 0.04 ($0 \le \varphi_2 \le 0.04$), while the volume fraction of Al_2O_3 is kept fixed at $\varphi_1 = 0.04$ and water as the base fluid. Table 3 provides the numerical values of $f''(1)$ and $-2\theta'(1)$ under different values of Re for regular fluid ($\varphi_1 = \varphi_2 = 0$) when $\varepsilon = 0$ and Pr $= 6.2$. In the present study, $\eta_\infty = 35$ is sufficient for the velocity and temperature profiles to reach the far-field boundary conditions asymptotically, which supports the validity of the numerical results. The increase of $f''(1)$ and $-2\theta'(1)$ are
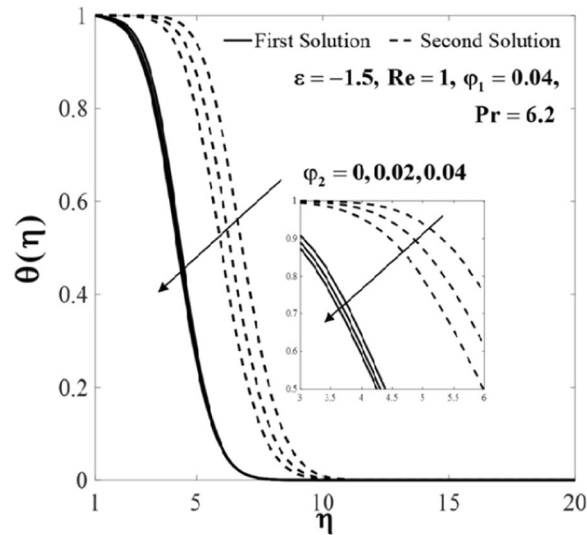
Figure 7. Plot of $\theta(\eta)_f$ for different values of φ_2.
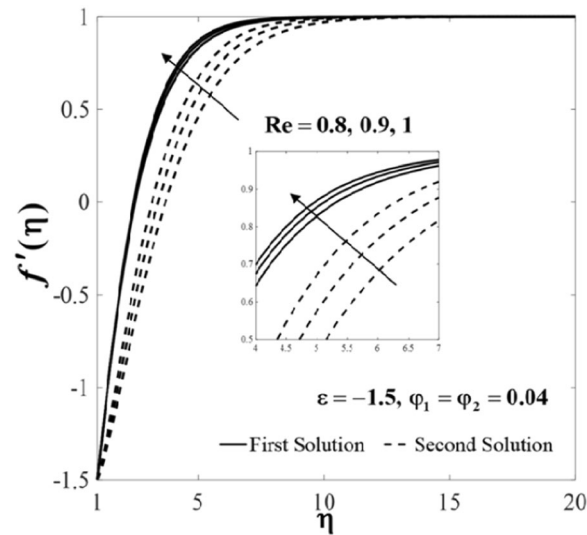
Figure 8. Plot of $f'(\eta)$ for different values of Re.

observed as *Re* increases. Also, the comparison values of $f''(1)$ with those of Wang[8,9] and Lok and Pop[12] are shown in the same table. It is observed that the comparison is in excellent agreement with the mentioned literature which supports the validity of the present numerical results. Additionally, Table 4 shows the effects of φ_2, *Re*, and ε on the skin friction coefficient $(Rez/a)C_f$ and the Nusselt number *Nu* for Cu/water ($\varphi_1 = 0$) and Al$_2$O$_3$-Cu/water ($\varphi_1 = 0.04$) when Pr = 6.2. It is observed that the values of $(Rez/a)C_f$ and *Nu* increase with the increasing values of φ_2 and *Re*. Besides, the values of $(Rez/a)C_f$ decrease, whereas *Nu* increases with increasing values of ε. Also, the heat transfer rate for Al$_2$O$_3$-Cu/water hybrid nanofluid is intensified if compared to Cu/water nanofluid.

The non-uniqueness of the solutions of Eqs. (6) to (8) is observed for some values of ε as can be seen in Figs. 2–5. For example, the variations of $(Rez/a)C_f$ and *Nu* against ε for several values of φ_1 and φ_2 when Re = 1 and Pr = 6.2 are displayed in Figs. 2 and 3. It is noticed that dual solutions are possible for $\varepsilon_c < \varepsilon < -1$, and the solution is unique for $\varepsilon \geq -1$. Besides, both branch solutions (first and second) merge up to certain critical values of ε, say ε_c. Here, $\varepsilon_{c1} = -1.54398$, $\varepsilon_{c2} = -1.54269$, and $\varepsilon_{c3} = -1.52549$ are the critical values for the case of regular fluid ($\varphi_1 = \varphi_2 = 0$), Al$_2O_3$/water nanofluid ($\varphi_1 = 0.04$, $\varphi_2 = 0$), and Al$_2$O$_3$-Cu/water hybrid nanofluid ($\varphi_1 = \varphi_2 = 0.04$), respectively. In addition, the Nusselt number *Nu* enhances for both stretching and shrinking cases in the presence of nanoparticles. However, the skin friction $(Rez/a)C_f$ increases for fixed values of ε started from $\varepsilon < 1$, but these values decrease for $\varepsilon > 1$ and zero skin friction is observed for $\varepsilon = 1$. Comparing the three types of fluid, it is found that these physical quantities are intensified for hybrid nanofluid compared to the others. The observation is consistent with the fact that the added hybrid nanoparticles have the capacity of raising the heat transfer rate because of the synergistic effects as discussed by Sarkar *et al.*[27].
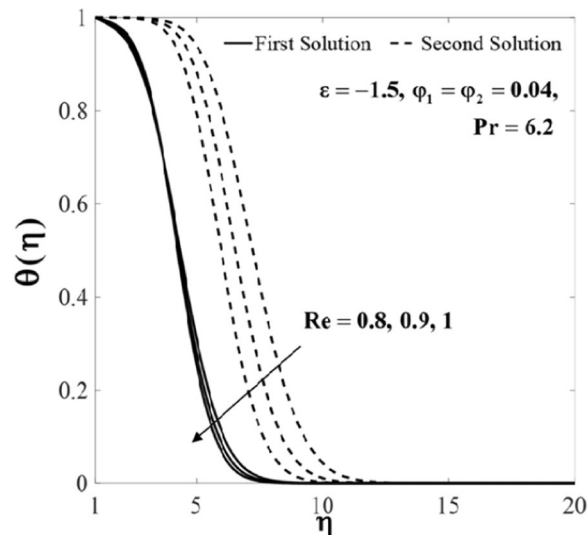
Figure 9. Plot of $\theta(\eta)$ for different values of Re.
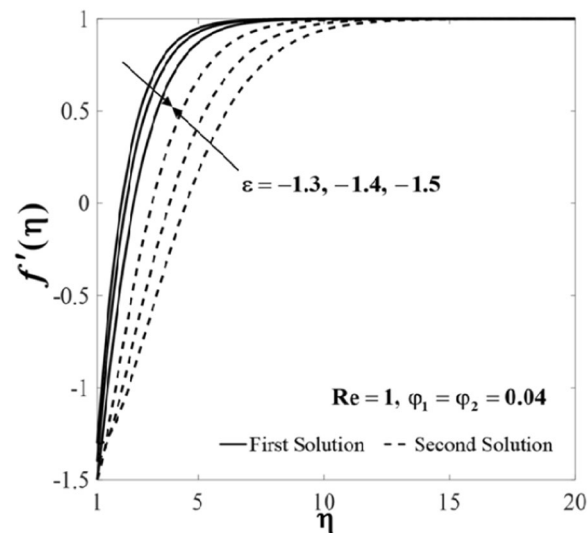
Figure 10. Plot of $f'(\eta)$ for different values of ε.

Figures 4 and 5 show the variations of the skin friction coefficient $(Re_z/a)C_f$ and the Nusselt number Nu against ε for several values of Re when $\varphi_1 = \varphi_2 = 0.04$ and Pr = 6.2. The effect of increasing Re has a similar trend if compared to the effect of nanoparticles on the skin friction $(Re_z/a)C_f$. Physically, Reynolds number Re indicates the relative significance of the inertia effect compared to the viscous effect. As expected, the skin friction coefficients (the surface shear-stress) increases for increasing values of the Reynolds number Re. The upsurge of Re has a tendency to enhance the Nusselt number Nu for $\varepsilon > -1.2$, and it decreases for $\varepsilon < -1.2$, where the heat transfer occurs almost at the same rate as $\varepsilon = -1.2$. Also, it is noticed that the increment is more dominant for the stretching case ($\varepsilon > 0$). Besides, the range of ε for which the solution is in existence decreases as Re increases. As shown in Figs. 4 and 5, the minimum values of ε for the solution to exist are $\varepsilon_{c1} = -1.76968$, $\varepsilon_{c2} = -1.61586$, and $\varepsilon_{c3} = -1.52549$ for Re = 0.2, 0.5, 1, respectively.

Further, the velocity profiles $f'(\eta)$ and the temperature profiles $\theta(\eta)$ for selected values of parameters are provided in Figs. 6–11. These profiles asymptotically satisfy the free stream conditions (8), and thus supports the validity of the numerical solutions. The increasing behaviour for both branch solutions of $f'(\eta)$ is observed with the increase of φ_2 when $\varepsilon = -1.5$, Re = 1, $\varphi_1 = 0.04$, and Pr = 6.2, however, the observation is reversed for $\theta(\eta)$ as can be seen in Figs. 6 and 7, respectively. Moreover, the effect of Re on $f'(\eta)$ and $\theta(\eta)$ when $\varepsilon = -1.5$, $\varphi_1 = \varphi_2 = 0.04$, and Pr = 6.2 are exhibited in Figs. 8 and 9. As predicted, the velocity $f'(\eta)$ increases with the rise of Reynolds number Re and as a result, the temperature $\theta(\eta)$ decreases once the thermal diffusion is overcome. This observation shows similar results as those of Lok and Pop[12] for the viscous fluid case. In addition, the effect of ε
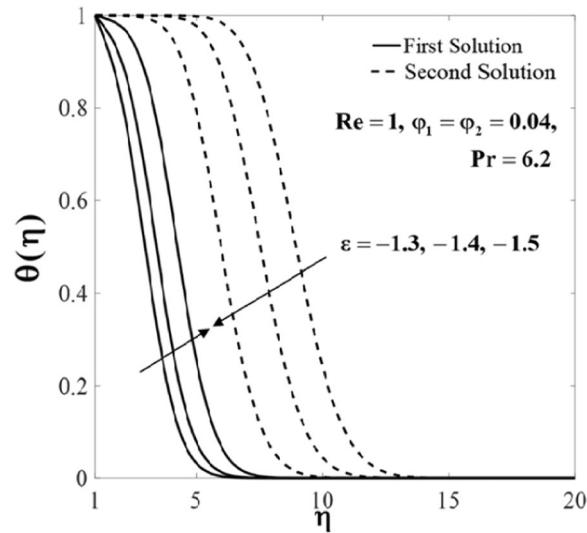
Figure 11. Plot of $\theta(\eta)$ for different values of ε.
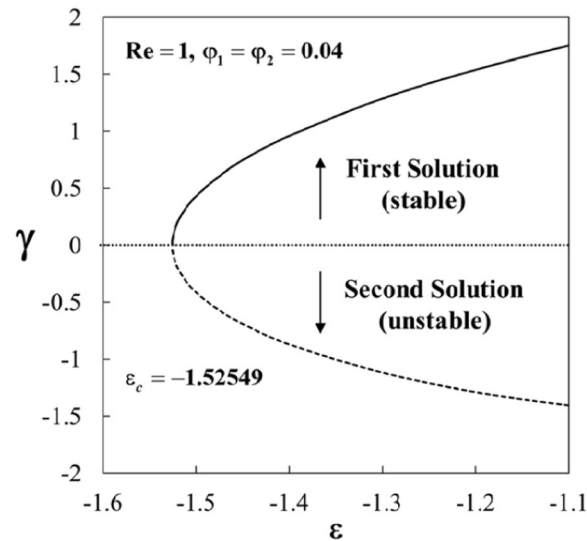
Figure 12. Plot of γ against ε for $F''(1) = 1$.

on $f'(\eta)$ and $\theta(\eta)$ when $\mathrm{Re} = 1$, $\varphi_1 = \varphi_2 = 0.04$, and $\mathrm{Pr} = 6.2$ are presented in Figs. 10 and 11. It can be predicted that both solutions merge at $\varepsilon = \varepsilon_c$. This observation is consistent with the results presented in Figs. 2–5.

The variations of the smallest eigenvalues γ against ε when $\varphi_1 = \varphi_2 = 0.04$ and $\mathrm{Re} = 1$ are portrayed in Fig. 12. It is noticed that the values of γ are positive for the first solution, while it is negative for the second solution. Also, the values of γ approach to zero for both solutions when $\varepsilon \to \varepsilon_c = -1.52549$. Thus, this finding confirms that the first solution is stable and physically reliable while the second solution is not. Besides, it is concluded that the bifurcation of the solutions happens at the critical (minimum) value $\varepsilon = \varepsilon_c$.

Equations (6) to (8) admit dual solutions due to the reverse flow occurs in the boundary layer induced by the shrinking sheet. The occurrence of this phenomenon creates the separation of the boundary layer where the flow moves in the opposite direction as shown in Fig. 1(b). The stability of the solutions is indicated by the sign of the eigenvalue γ. As described in Eq. (15), there is an initial decay of disturbance when $\gamma > 0$ as time evolves, i.e. $e^{-\gamma\tau} \to 0$ as $\tau \to \infty$. Thus, the flow is stable in the long run when $\gamma > 0$. In contrast, the flow is unstable when $\gamma < 0$ since $e^{-\gamma\tau} \to \infty$ as $\to \infty$. The latter shows an increase of disturbance as time evolves. This analysis shows that the first solutions are stable and thus physically reliable in the long run, while the second solutions are not and have no physical sense. Although such solutions are deprived of physical significance, they are nevertheless of interest so far as the differential equations are concerned. These solutions are of mathematical interest since they are also solutions to the differential equations. Similar equations may arise in other situations where the corresponding solutions could have more realistic meaning[56].

Conclusion

In the present study, the hybrid nanofluid flow towards a stagnation point on a stretching/shrinking cylinder has been accomplished. The results were obtained through the bvp4c solver in Matlab software. The results validation was done for limiting cases where the current results were found to compare well with the existing results. The effects of the nanoparticles volume fractions (φ_1 and φ_2), stretching/shrinking parameter ε, and Reynolds number Re on the flow and heat transfer characteristics have been examined. From this investigation, we can draw the following conclusions:

- The findings revealed that the heat transfer rate improved in the presence of hybrid nanoparticles.
- It was found that dual solutions are possible for certain physical parameters, where the bifurcation of the solutions occurred in the shrinking region ($\varepsilon < 0$).
- The Nusselt number Nu enhanced with increasing values of the Reynolds number Re. The effect of Re was more dominant for the case of the stretching surface ($\varepsilon > 0$).
- The velocity increased, but the temperature decreased with the rising of φ_2 and Re.
- Between the two solutions, only one of them is stable and physically reliable, while the other is unstable as time evolved.

References

1. Fisher, E. G. *Extrusion of Plastics*. (Wiley, New York, 1976).
2. Tadmor, Z. & Klein, I. *Engineering Principles of Plasticating Extrusion*. (Van Nostrand Reinhold Inc, U.S, 1970).
3. Crane, L. J. Flow past a stretching plate. *Zeitschrift Für Angew. Math. Und Phys. ZAMP* **21**, 645–647 (1970).
4. Goldstein, S. On backward boundary layers and flow in converging passages. *J. Fluid Mech.* **21**, 33–45 (1965).
5. Wang, C. Y. Liquid film on an unsteady stretching surface. *Q. Appl. Math.* **48**, 601–610 (1990).
6. Miklavčič, M & Wang, C. Y. Viscous flow due to a shrinking sheet. *Q. Appl. Math.* **64**, 283–290 (2006).
7. Wang, C. Y. Stagnation flow towards a shrinking sheet. *Int. J. Non. Linear. Mech.* **43**, 377–382 (2008).
8. Wang, C. Axisymmetric stagnation flow on a cylinder. *Q. Appl. Math.* **32**, 207–213 (1974).
9. Wang, C. Y. Stagnation flow on a cylinder with partial slip-an exact solution of the Navier-Stokes equations. *IMA J. Appl. Math. (Institute Math. Its Appl.)* **72**, 271–277 (2007).
10. Gorla, R. S. R. Heat transfer in an axisymmetric stagnation flow on a cylinder. *Appl. Sci. Res.* **32**, 541–553 (1976).
11. Cunning, G. M., Davis, A. M. J. & Weidman, P. D. Radial stagnation flow on a rotating circular cylinder with uniform transpiration. *J. Eng. Math.* **33**, 113–128 (1998).
12. Lok, Y. Y. & Pop, I. Wang's shrinking cylinder problem with suction near a stagnation point. *Phys. Fluids* **23**, 083102 (2011).
13. Merkin, J. H., Najib, N., Bachok, N., Ishak, A. & Pop, I. Stagnation-point flow and heat transfer over an exponentially stretching/shrinking cylinder. *J. Taiwan Inst. Chem. Eng.* **74**, 65–72 (2017).
14. Zaimi, W. M. K. A. W., Ishak, A. & Pop, I. Unsteady viscous flow over a shrinking cylinder. *J. King Saud Univ. - Sci.* **25**, 143–148 (2013).
15. Soomro, F. A., Zaib, A., Haq, R. U. & Sheikholeslami, M. Dual nature solution of water functionalized copper nanoparticles along a permeable shrinking cylinder: FDM approach. *Int. J. Heat Mass Transf.* **129**, 1242–1249 (2019).
16. Ishak, A., Nazar, R. & Pop, I. Magnetohydrodynamic (MHD) flow and heat transfer due to a stretching cylinder. *Energy Convers. Manag.* **49**, 3265–3269 (2008).
17. Fang, T. G., Zhang, J., Zhong, Y. F. & Tao, H. Unsteady viscous flow over an expanding stretching cylinder. *Chinese Phys. Lett.* **28**, 124707 (2011).
18. Fang, T., Zhang, J. & Zhong, Y. Note on unsteady viscous flow on the outside of an expanding or contracting cylinder. *Commun. Nonlinear Sci. Numer. Simul.* **17**, 3124–3128 (2012).
19. Ahmed, S. E., Hussein, A. K., Mohammed, H. A. & Sivasankaran, S. Boundary layer flow and heat transfer due to permeable stretching tube in the presence of heat source/sink utilizing nanofluids. *Appl. Math. Comput.* **238**, 149–162 (2014).
20. Pandey, A. K. & Kumar, M. Boundary layer flow and heat transfer analysis on Cu-water nanofluid flow over a stretching cylinder with slip. *Alexandria Eng. J.* **56**, 671–677 (2017).
21. Mohammadiun, H., Amerian, V., Mohammadiun, M. & Rahimi, A. B. Similarity solution of axisymmetric stagnation-point flow and heat transfer of a nanofluid on a stationary cylinder with constant wall temperature. *Iran. J. Sci. Technol. - Trans. Mech. Eng.* **41**, 91–95 (2017).
22. Choi, S. U. S. & Eastman, J. A. Enhancing thermal conductivity of fluids with nanoparticles. *Proc. 1995 ASME Int. Mech. Eng. Congr. Expo. FED 231/MD* 99–105, https://doi.org/10.1115/1.1532008 (1995).
23. Khanafer, K., Vafai, K. & Lightstone, M. Buoyancy-driven heat transfer enhancement in a two-dimensional enclosure utilizing nanofluids. *Int. J. Heat Mass Transf.* **46**, 3639–3653 (2003).
24. Oztop, H. F. & Abu-Nada, E. Numerical study of natural convection in partially heated rectangular enclosures filled with nanofluids. *Int. J. Heat Fluid Flow* **29**, 1326–1336 (2008).
25. Turcu, R. *et al.* New polypyrrole-multiwall carbon nanotubes hybrid materials. *J. Optoelectron. Adv. Mater.* **8**, 643–647 (2006).
26. Jana, S., Salehi-Khojin, A. & Zhong, W. H. Enhancement of fluid thermal conductivity by the addition of single and hybrid nano-additives. *Thermochim. Acta* **462**, 45–55 (2007).
27. Sarkar, J., Ghosh, P. & Adil, A. A review on hybrid nanofluids: Recent research, development and applications. *Renew. Sustain. Energy Rev.* **43**, 164–177 (2015).
28. Devi, S. P. A. & Devi, S. S. U. Numerical investigation of hydromagnetic hybrid Cu- Al2O3/water nanofluid flow over a permeable stretching sheet with suction. *Int. J. Nonlinear Sci. Numer. Simul.* **17**, 249–257 (2016).
29. Devi, S. S. U. & Devi, S. P. A. Numerical investigation of three-dimensional hybrid Cu–Al2O3/water nanofluid flow over a stretching sheet with effecting Lorentz force subject to Newtonian heating. *Can. J. Phys.* **94**, 490–496 (2016).
30. Suresh, S., Venkitaraj, K. P., Selvakumar, P. & Chandrasekar, M. Synthesis of Al2O3-Cu/water hybrid nanofluids using two step method and its thermo physical properties. *Colloids Surfaces A Physicochem. Eng. Asp.* **388**, 41–48 (2011).
31. Waini, I., Ishak, A. & Pop, I. Unsteady flow and heat transfer past a stretching/shrinking sheet in a hybrid nanofluid. *Int. J. Heat Mass Transf.* **136**, 288–297 (2019).
32. Waini, I., Ishak, A. & Pop, I. Flow and heat transfer along a permeable stretching/shrinking curved surface in a hybrid nanofluid. *Phys. Scr.* **94**, 105219 (2019).

33. Waini, I., Ishak, A. & Pop, I. Hybrid nanofluid flow and heat transfer over a nonlinear permeable stretching/shrinking surface. *Int. J. Numer. Methods Heat Fluid Flow* **29**, 3110–3127 (2019).
34. Waini, I., Ishak, A. & Pop, I. Hybrid nanofluid flow and heat transfer past a vertical thin needle with prescribed surface heat flux. *Int. J. Numer. Methods Heat Fluid Flow* **29**, 4875–4894 (2019).
35. Waini, I., Ishak, A. & Pop, I. Transpiration effects on hybrid nanofluid flow and heat transfer over a stretching/shrinking sheet with uniform shear flow. *Alexandria Eng. J.* **59**, 91–99 (2020).
36. Waini, I., Ishak, A. & Pop, I. Hybrid nanofluid flow induced by an exponentially shrinking sheet. *Chinese J. Phys*. https://doi.org/10.1016/j.cjph.2019.12.015 (2019).
37. Waini, I., Ishak, A. & Pop, I. MHD flow and heat transfer of a hybrid nanofluid past a permeable stretching/shrinking wedge. *Appl. Math. Mech. (English Ed.)* **41**, 507–520 (2020).
38. Lund, L. A., Omar, Z., Raza, J. & Khan, I. Magnetohydrodynamic flow of Cu–Fe$_3$O$_4$/H$_2$O hybrid nanofluid with effect of viscous dissipation: Dual similarity solutions. *J. Therm. Anal. Calorim*., https://doi.org/10.1007/s10973-020-09602-1 (2020).
39. Lund, L. A. *et al*. Stability analysis and multiple solution of Cu-Al$_2$O$_3$/H$_2$O nanofluid contains hybrid nanomaterials over a shrinking surface in the presence of viscous dissipation. *J. Mater. Res. Technol.* **9**, 421–432 (2020).
40. Lund, L. A., Omar, Z., Khan, I. & Sherif, E. S. M. Dual solutions and stability analysis of a hybrid nanofluid over a stretching/shrinking sheet executing MHD flow. *Symmetry* **12**, 276, https://doi.org/10.3390/sym12020276 (2020).
41. Khan, M. R., Pan, K., Khan, A. U. & Nadeem, S. Dual solutions for mixed convection flow of SiO2−Al2O3/water hybrid nanofluid near the stagnation point over a curved surface. *Phys. A Stat. Mech. its Appl.* **547**, 123959, https://doi.org/10.1016/j.physa.2019.12395 (2020).
42. Khan, U., Zaib, A., Khan, I., Baleanu, D. & Nisar, K. S. Enhanced heat transfer in moderately ionized liquid due to hybrid MoS2/SiO2 nanofluids exposed by nonlinear radiation: Stability analysis. *Crystals* **10**, 142, https://doi.org/10.3390/cryst10020142 (2020).
43. Khashi'ie, N. S. *et al*. Magnetohydrodynamics (MHD) axisymmetric flow and heat transfer of a hybrid nanofluid past a radially permeable stretching/shrinking sheet with Joule heating. *Chinese J. Phys.* **64**, 251–263 (2020).
44. Aly, E. H. & Pop, I. MHD flow and heat transfer over a permeable stretching/shrinking sheet in a hybrid nanofluid with a convective boundary condition. *Int. J. Numer. Methods Heat Fluid Flow* **29**, 3012–3038 (2019).
45. Hayat, T., Nadeem, S. & Khan, A. U. Rotating flow of Ag-CuO/H$_2$O hybrid nanofluid with radiation and partial slip boundary effects. *Eur. Phys. J. E* **41**, 75 (2018).
46. Merkin, J. H. On dual solutions occurring in mixed convection in a porous medium. *J. Eng. Math.* **20**, 171–179 (1986).
47. Weidman, P. D., Kubitschek, D. G. & Davis, A. M. J. The effect of transpiration on self-similar boundary layer flow over moving surfaces. *Int. J. Eng. Sci.* **44**, 730–737 (2006).
48. Harris, S. D., Ingham, D. B. & Pop, I. Mixed convection boundary-layer flow near the stagnation point on a vertical surface in a porous medium: Brinkman model with slip. *Transp. Porous Media* **77**, 267–285 (2009).
49. Shampine, L. F., Gladwell, I. & Thompson, S. *Solving ODEs with MATLAB*. (Cambridge University Press, Cambridge, 2003).
50. Awaludin, I. S., Ishak, A. & Pop, I. On the stability of MHD boundary layer flow over a stretching/shrinking wedge. *Sci. Rep.* **8**, 13622 (2018).
51. Soid, S. K., Ishak, A. & Pop, I. MHD stagnation-point flow over a stretching/shrinking sheet in a micropolar fluid with a slip boundary. *Sains Malays* **47**, 2907–2916 (2018).
52. Kamal, F., Zaimi, K., Ishak, A. & Pop, I. Stability analysis of MHD Stagnation-point flow towards a permeable stretching/shrinking sheet in a nanofluid with chemical reactions effect. *Sains Malays* **48**, 243–250 (2019).
53. Waini, I., Ishak, A. & Pop, I. On the stability of the flow and heat transfer over a moving thin needle with prescribed surface heat flux. *Chinese J. Phys.* **60**, 651–658 (2019).
54. Zaib, A., Khan, M. & Shafie, S. Boundary layer flow of a copper-water nanofluid over a permeable shrinking cylinder with homogenous-hetrogenous reactions: Dual solutions. *Therm. Sci.* **23**, 295–306 (2019).
55. Khan, U., Zaib, A., Khan, I. & Nisar, K. S. Activation energy on MHD flow of titanium alloy (Ti6Al4V) nanoparticle along with a cross flow and streamwise direction with binary chemical reaction and non-linear radiation: Dual solutions. *J. Mater. Res. Technol.* **9**, 188–199 (2020).
56. Rhida, A. Aiding flows non-unique similarity solutions of mixed-convection boundary-layer equations. *Z. angew. Math. Phys.* **47**, 341–352 (1996).

Acknowledgements

Author contributions

I.W. and A.I. performed the numerical analysis and wrote the manuscript. I.P. carried out the literature review and co-wrote the manuscript.

Competing interests

The authors declare no competing interests.

Additional information

Correspondence and requests for materials should be addressed to A.I.

Reprints and permissions information is available at www.nature.com/reprints.

Publisher's note Springer Nature remains neutral with regard to jurisdictional claims in published maps and institutional affiliations.